

Ab initio calculations of phonon spectra in $ATiO_3$ perovskite crystals ($A = Ca, Sr, Ba, Ra, Cd, Zn, Mg, Ge, Sn, Pb$)

Alexander I. Lebedev*

Physics Department, Moscow State University, 119991 Moscow, Russia

(Dated: October 30, 2018)

The phonon spectra of calcium, strontium, barium, radium, cadmium, zinc, magnesium, germanium, tin, and lead titanates with the perovskite structure are calculated from first principles within the density functional theory. By analyzing the unstable modes in the phonon spectra, the possible lattice distortions are determined and the energies of the corresponding phases are calculated. From analyzing the phonon spectra, force constants, and eigenvectors of TO phonons, a conclusion is drawn on the origin of the ferroelectricity in considered crystals. It is shown that the main factors determining the possible off-centering of atoms in the A position are the geometric size and electronic configuration of these atoms.

DOI: 10.1134/S1063783409020279

PACS numbers: 61.50.Ah 63.20.Dj 71.15.Mb 77.84.Dy

I. INTRODUCTION

Crystals of the perovskite family are well-known materials undergoing various structural distortions with decreasing temperature. When the character of these distortions is ferroelectric, a number of physical properties of these crystals (dielectric constant, piezoelectric coefficients, etc.) becomes anomalously large. For this reason, these materials have found wide application in modern electronics.

The problem of further optimization of the ferroelectric properties requires a deeper understanding of the microscopic mechanisms responsible for the appearance of ferroelectricity and the ferroelectric properties. In solving this problem, very useful information can be obtained from the *ab initio* calculations which have already made a significant contribution to the understanding of the ferroelectric phenomena in the perovskite crystals.¹⁻¹¹

In discussing the properties of ferroelectrics, it is very important to understand whether these properties result from a collective displacement of atoms in a lattice (displacive phase transition) or they are due to specific features of certain constituent atoms in a crystal (order-disorder phase transition). This problem arises, in particular, in discussing the nature of the phase transitions that occur in incipient ferroelectrics doped with certain impurities.¹²

Earlier studies of titanates with the perovskite structure have dealt mainly with four compounds ($CaTiO_3$,^{3,4,13,14} $SrTiO_3$,^{3,4,6} $BaTiO_3$,^{1-4,8,9} and $PbTiO_3$ ^{2-4,7,9}) and their solid solutions. However, a comparison of the results obtained in these studies is hampered by different calculation techniques used in these investigations and different methods used to construct atomic (pseudo)potentials.

The aim of this work is to carry out first-principles calculations of the phonon spectra of ten $ATiO_3$ crystals with the perovskite structure and determine the structure of the most stable phases. In order to test our approach, we first apply it for calculating the properties

of the four above-mentioned systems. Then we predict the properties of poorly investigated or hypothetical perovskite compounds $RaTiO_3$, $CdTiO_3$, $MgTiO_3$, $ZnTiO_3$, $SnTiO_3$, and $GeTiO_3$.¹⁵ From comparison of the results obtained in a unified way for a large number of related materials, conclusions are made about the relation of the structural distortions in $ATiO_3$ crystals to the size and electronic structure of the A atom. From the analysis of the on-site force-constant matrix and the TO-phonon eigenvectors, we draw conclusions about the origin of the ferroelectricity in these materials and find conditions under which the ferroelectric phenomena can be associated with off-center atoms.

II. CALCULATION TECHNIQUE

The calculations were performed using the ABINIT software¹⁶ based on the density functional theory, pseudopotentials, and the plane-wave expansion of the wave functions. The exchange-correlation interaction was described in the local density approximation (LDA).¹⁷ The used pseudopotentials were optimized separable nonlocal pseudopotentials,¹⁸ which were constructed using the OPIUM code and to which the local potential correction¹⁹ was added in order to improve their transferability. For elements with atomic numbers $Z < 46$, the construction was performed in a non-relativistic way; for other elements, a scalar-relativistic approximation was used. Table I lists the parameters used for constructing pseudopotentials. The local potential was the s potential except for the oxygen atom, for which the local d potential was used. The parameters of pseudopotentials were finely adjusted by comparing the calculated and experimental values of the lattice parameters for a number of oxides and sulfides of the elements.

The lattice parameters and the equilibrium atomic positions in the unit cell were obtained by minimizing the Hellmann-Feynman forces acting on the atoms ($<10^{-5}$ Ha/Bohr), with the total energy being calculated self-

consistently with an accuracy of better than 10^{-10} Ha.²⁰ In the calculations, particular attention was paid to the convergence of the results with respect to the kinetic energy cut-off for plane waves and the density of the k -point mesh used in the integration over the Brillouin zone. For all the calculated properties presented below, the convergence was attained at an energy cut-off of 30 Ha and the $8 \times 8 \times 8$ k -point mesh constructed according to Ref. 21.

The Born effective charges Z^* , optical dielectric constant ϵ_∞ , elastic moduli C_{ij} , bulk modulus B , force-constant matrix Φ_{ij} , and phonon spectra were calculated using the density-functional perturbation theory.^{22–25} The phonon frequencies were calculated exactly at five points of the Brillouin zone (Γ , X , M , R , and the Λ point located halfway between the Γ and R points), and then the phonon spectrum was computed over the entire Brillouin zone using the interpolation technique.^{22,26}

III. TESTING OF THE CALCULATION TECHNIQUE

The correctness of the described approach was tested by comparing the calculated lattice parameters, spontaneous polarizations, and phonon spectra with available experimental data and calculations performed by other authors for well-studied CaTiO_3 , SrTiO_3 , BaTiO_3 , and PbTiO_3 compounds.

The lattice parameters corresponding to a minimum total energy of the crystals are given in Table II. The obtained values agree well with the experimental data²⁷ if one takes into account that the LDA usually slightly underestimates the lattice parameter. An analysis of the relative energies (per formula unit) of low-symmetry phases (Table III) shows that for barium titanate, the most energetically favorable phase is the rhombohedral one and for lead titanate, it is the tetragonal phase. The calculated values of the c/a ratio for tetragonal BaTiO_3 and PbTiO_3 are close to the experimental values (Table II). For CaTiO_3 , the most energetically favorable phase is the orthorhombic $Pbnm$ phase and for SrTiO_3 , it is the tetragonal $I4/mcm$ phase. The values of spontaneous polarization calculated by the Berry phase method²⁸ are 0.26, 0.31, and 0.89 C/m² for tetragonal BaTiO_3 , rhombohedral BaTiO_3 , and tetragonal PbTiO_3 , respectively. These values are close to the experimental data (0.26, 0.33, 0.75 C/m², Ref. 27).

The calculated optical-phonon frequencies are also in good agreement with available experimental data and calculations performed by other authors (Tables IV, V). The imaginary frequencies in Tables IV and V correspond to unstable modes, the squares of whose frequencies are negative.

The good agreement of our calculations with the experimental data and the calculations of other authors for CaTiO_3 , SrTiO_3 , BaTiO_3 , and PbTiO_3 suggests that the proposed approach can be used to predict the properties of poorly studied and hypothetical³¹ titanates with the

perovskite structure and to discuss the factors causing the appearance of ferroelectricity in them. The properties of these crystals calculated for the theoretical lattice parameter (i.e., the value corresponding to a minimum of the total energy) are given in Tables III to VII. Table III presents the energies of different low-symmetry phases measured relative to the energy of the parent cubic phase. Table IV gives the frequencies of optical phonons (three infrared-active Γ_{15} modes and one infrared-inactive Γ_{25} mode) in the cubic phase. Table V gives the lowest phonon frequencies at high-symmetry points of the Brillouin zone. The values of the Born effective charges and optical dielectric constants for the cubic phase of ATiO_3 compounds are given in Table VI. Finally, the elastic moduli of several crystals are presented in Table VII.

The phonon dispersion curves along some high-symmetry directions calculated for the cubic phase of ten titanates are shown in Fig. 1. The imaginary phonon frequencies associated with the structural instability of the crystals are represented in Fig. 1 by negative values.

IV. RESULTS

As follows from Fig. 1, unstable optical modes of different symmetry are present in the phonon spectra of all studied titanates. At first, we discuss the phonon spectra of well-studied compounds.

A specific feature of the dispersion curves of SrTiO_3 is that among three unstable phonons at the Γ , R , and M points, the most unstable phonon is that at the R point (the R_{25} mode)³² and that the phonon frequency depends only weakly on the wave vector along the R - M line. As shown in Ref. 6, in the real space, these unstable phonons with the wave vectors near the edges of the cubic Brillouin zone correspond to the rotation of the oxygen octahedra linked together by shared vertices, with the correlation length for rotations being three to five lattice periods. Thus, the R_{25} mode and the M_3 mode (which corresponds to the unstable phonon at the M point) describe the structural distortions associated with the rotation of the octahedra. The unstable Γ_{15} phonon mode at the Γ point corresponds to the ferroelectric distortion of the structure.

The R_{25} mode is triply degenerate, and the distortions described by the three-component order parameters $(\eta, 0, 0)$, $(\eta, \eta, 0)$, and (η, η, η) lead to low-symmetry phases with the space groups $I4/mcm$, $Imma$, and $R3c$, respectively. The M_3 mode is nondegenerate, and its condensation lowers the crystal symmetry to $P4/mbm$. The triply degenerate Γ_{15} mode results in the well-known space groups $P4mm$, $Amm2$, and $R3m$. From comparing the energies of these phases (Table III), it follows that the lowest-energy phase in SrTiO_3 is the $I4/mcm$ one, into which strontium titanate transforms with decreasing temperature. The instability of the ferroelectric mode in this compound is not sufficiently strong for ferroelectricity to occur.

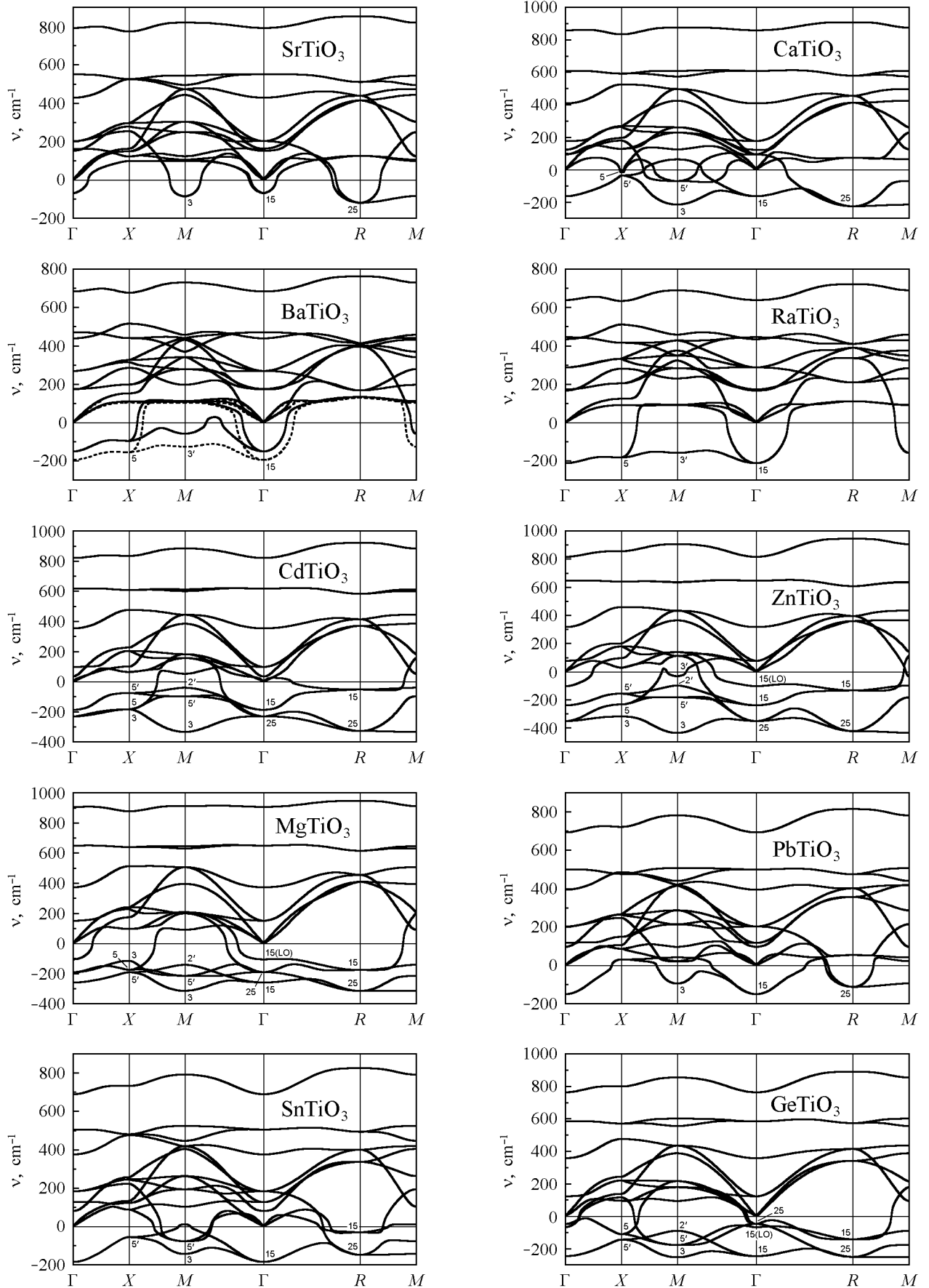


FIG. 1. Phonon dispersion curves for the cubic phase of $ATiO_3$ compounds. The labels indicate the symmetry of unstable modes.

TABLE I. Electronic configurations of atoms and parameters used to construct pseudopotentials: r_s , r_p , and r_d are the core radii of the pseudopotentials for the s , p , and d projections; q_s , q_p , and q_d are the cut-off wave vectors used to optimize pseudopotentials; and r_{\min} , r_{\max} , and V_{loc} are the limits and the depth of the correcting local potential (parameter values are in atomic units, and energy is given in Ry).

Atom	Configuration	r_s	r_p	r_d	q_s	q_p	q_d	r_{\min}	r_{\max}	V_{loc}
Ca	$3s^2 3p^6 3d^0 4s^0$	1.46	1.68	1.82	7.07	7.07	7.27	0.01	1.40	1.6
Sr	$4s^2 4p^6 4d^0 5s^0$	1.68	1.74	1.68	7.07	7.07	7.07	0.01	1.52	1.5
Ba	$5s^2 5p^6 5d^0 6s^0$	1.85	1.78	1.83	7.07	7.07	7.07	0.01	1.68	1.95
Ra	$6s^2 6p^6 7s^0 6d^0 7p^0$	1.84	1.73	1.98	7.8	7.8	7.8	0.01	1.68	-1.3
Mg	$2s^2 2p^6 3s^0 3p^0$	1.50	1.88	—	6.7	8.1	—	0.01	1.0	-0.84
Zn	$3d^{10} 4s^0 4p^0$	1.82	1.82	2.00	7.07	7.07	7.47	0.01	1.60	2.5
Cd	$4d^{10} 5s^0 5p^0$	2.04	2.18	2.10	7.07	7.07	7.07	0	1.88	-1.6
Ge	$3d^{10} 4s^{1.5} 4p^{0.5}$	1.68	1.68	1.96	7.07	6.0	7.77	0.01	1.58	0.48
Sn	$4d^{10} 5s^2 5p^0$	2.14	2.08	2.18	7.07	7.07	7.07	0.01	1.90	0.64
Pb	$5d^{10} 6s^2 6p^0$	1.72	1.98	1.80	6.05	5.52	7.17	0.1	1.43	1.6
Ti	$3s^2 3p^6 3d^0 4s^0$	1.48	1.72	1.84	7.07	7.07	7.07	0.01	1.41	2.65
O	$2s^2 2p^4 3d^0$	1.40	1.55	1.40	7.07	7.57	7.07	—	—	—

TABLE II. Comparison of calculated and experimental lattice parameters of different phases of $ATiO_3$ compounds (experimental data are obtained at 300 K, unless otherwise specified).

Compound	Space group	Source	Lattice parameters
CaTiO ₃	<i>Pbnm</i>	This work	$a = 5.3108, b = 5.4459, c = 7.5718 \text{ \AA}$
		Exp. ²⁷	$a = 5.3670, b = 5.4439, c = 7.6438 \text{ \AA}$
SrTiO ₃	<i>Pm3m</i>	This work	$a = 3.8898 \text{ \AA}$
	<i>I4/mcm</i>	Exp. ²⁷	$a = 3.905 \text{ \AA}$
		This work	$a = b = 5.4680, c = 7.8338 \text{ \AA}$
BaTiO ₃	<i>Pm3m</i>	Exp. ²⁷	$a = b = 5.510, c = 7.798 \text{ \AA} (20 \text{ K})$
		This work	$a = 3.9721 \text{ \AA}$
	<i>P4mm</i>	Exp. ²⁷	$a = 3.996 \text{ \AA} (393 \text{ K})$
		This work	$a = 3.9650, c = 4.0070 \text{ \AA}, c/a = 1.0106$
		Exp. ²⁷	$a = 3.9920, c = 4.0361 \text{ \AA} (293 \text{ K})$
	<i>R3m</i>	This work	$a = 3.9620, b = 5.6384, c = 5.6484 \text{ \AA}$
Exp. ²⁷		$a = 3.990, b = 5.669, c = 5.682 \text{ \AA} (263 \text{ K})$	
PbTiO ₃	<i>P4mm</i>	This work	$a = 3.9817 \text{ \AA}, \alpha = 89.933^\circ$
		Exp. ²⁷	$a = 4.001 \text{ \AA}, \alpha = 89.85^\circ (105 \text{ K})$
		This work	$a = 3.8858, c = 4.1151 \text{ \AA}, c/a = 1.0590$
		Exp. ²⁷	$a = 3.904, c = 4.152 \text{ \AA}$

In CaTiO₃, in addition to the instabilities found above, three weak antiferroelectric-type instabilities associated with the X_5 , X'_5 , and M'_5 modes arise and the R - M segment of the phonon spectrum becomes practically dispersionless (compare mode energies in Table V). In the latter case, as shown by theoretical calculations,¹⁴ the simultaneous condensation of two unstable R_{25} and M_3 modes results in the formation of the *Pbnm* phase having the lowest energy among the possible distorted phases (Table III).³³ The transition from the high-temperature *Pm3m* phase to the low-temperature *Pbnm* phase can occur through one of three intermediate phases (*P4/mbm*, *I4/mcm*, and $R\bar{3}c$), whose energies are 0.11–

0.17 eV higher than the energy of the *Pbnm* phase.³⁴ The ferroelectric *P4mm* and *R3m* phases in CaTiO₃ have much higher energies and never arise. As for the weakly unstable X'_5 , X_5 , and M'_5 modes, they are doubly degenerate and the distortions described by the order parameters $(\eta, 0)$ and (η, η) result in the *Pmma*, *Cmcm*, and *Cmmm* phases. The energy gain resulting from the transformation into these phases, however, does not exceed 7 meV.

The phonon spectrum of BaTiO₃ significantly differs from the spectra discussed above by the absence of instability at the R point and the appearance of highly unstable X_5 and M'_3 modes (at the X and M points,

TABLE III. Relative energies of different low-symmetry phases of $ATiO_3$ compounds (energies of the most stable phases are in boldface).

Compound	Unstable mode	Space group	Energy (meV)	Unstable mode	Space group	Energy (meV)	Unstable mode	Space group	Energy (meV)
MgTiO ₃	Γ_{25}	$P\bar{4}m2$	-125 ^a	M'_5	$Cmmm$	-417 ^a	Γ_{15}, Γ_{25}	$Amm2$	-1380 ^a
	X_3	$P4_2/mmc$	-147 ^a	X'_5	$Pmma$	-500	$R_{25} + M_3$	$Cmcm$	-1658 ^a
	R_{15}	$I4/mmm$	-228 ^a	Γ_{25}	$R32$	-686 ^a	R_{25}	$R\bar{3}c$	-1727
	R_{15}	$R\bar{3}m$	-289 ^a	Γ_{15}	$R3m$	-695	R_{15}, R_{25}	$Imma$	-1764 ^a
	X'_5	$Cmcm$	-304	Γ_{15}	$P4mm$	-1028	$R_{25} + M_3$	$Pbnm$	-1992
	M'_5	$Pmma$	-344 ^a	M_3	$P4/mbm$	-1107			
	M'_2	$P4/nmm$	-417 ^a	R_{25}	$I4/mcm$	-1111			
CaTiO ₃	X_5	$Cmcm$	-0.0 ^a	M'_5	$Cmmm$	-6.7	R_{25}	$I4/mcm$	-365
	X_5	$Pmma$	-0.0 ^a	Γ_{15}	$R3m$	-73.7	R_{25}	$R\bar{3}c$	-385
	X'_5	$Cmcm$	-0.6	Γ_{15}	$Amm2$	-85.4 ^a	$R_{25} + M_3$	$Cmcm$	-404 ^a
	X'_5	$Pmma$	-0.9	Γ_{15}	$P4mm$	-123	R_{25}	$Imma$	-412 ^a
	M'_5	$Pmma$	-5.0	M_3	$P4/mbm$	-321	$R_{25} + M_3$	$Pbnm$	-497
SrTiO ₃	Γ_{15}	$P4mm$	-0.71	M_3	$P4/mbm$	-9.45	R_{25}	$I4/mcm$	-30.9
	Γ_{15}	$Amm2$	-0.75 ^a	R_{25}	$R\bar{3}c$	-27.5			
	Γ_{15}	$R3m$	-0.75	R_{25}	$Imma$ ^b	-28.9			
BaTiO ₃	M'_3	$P4/nmm$	-0.31	X_5	$Cmcm$	-1.45	Γ_{15}	$Amm2$	-7.4
	X_5	$Pmma$	-1.22	Γ_{15}	$P4mm$	-5.6	Γ_{15}	$R3m$	-8.1
RaTiO ₃	M'_3	$P4/nmm$	-11.1	X_5	$Cmcm$	-16.9	Γ_{15}	$Amm2$	-28.5
	X_5	$Pmma$	-14.2	Γ_{15}	$P4mm$	-21.8	Γ_{15}	$R3m$	-29.7
CdTiO ₃	R_{15}	$I4/mmm$	-24 ^a	X_5	$Pmma$	-160	R_{25}	$I4/mcm$	-912
	R_{15}	$R\bar{3}m$	-30 ^a	Γ_{15}	$R3m$	-245	M_3	$P4/mbm$	-920
	X_3	$P4_2/mmc$	-45	X_5	$Cmcm$	-282	$R_{25} + M_3$	$Cmcm$	-1157 ^a
	X'_5	$Cmcm$	-66 ^a	Γ_{15}	$P4mm$	-340	R_{25}	$R\bar{3}c$	-1197
	X'_5	$Pmma$	-104 ^a	Γ_{15}, Γ_{25}	$Amm2$	-412	R_{15}, R_{25}	$Imma$	-1202 ^a
	Γ_{25}	$P\bar{4}m2$	-134	Γ_{25}	$R32$	-486	$R_{25} + M_3$	$Pbnm$	-1283
ZnTiO ₃	X_3	$P4_2/mmc$	-171 ^a	M'_5	$Cmmm$	-564 ^a	R_{25}	$I4/mcm$	-1443
	Γ_{25}	$P\bar{4}m2$	-341	M'_2	$P4/nmm$	-688 ^a	M_3	$P4/mbm$	-1449
	R_{15}	$I4/mmm$	-375 ^a	X'_5	$Pmma$	-752 ^a	Γ_{25}	$R32$	-1486
	X_5	$Pmma$	-447	X_5	$Cmcm$	-867	$R_{25} + M_3$	$Cmcm$	-2036 ^a
	X'_5	$Cmcm$	-449 ^a	Γ_{15}	$R3m$	-868	R_{15}, R_{25}	$Imma$	-2215 ^a
	R_{15}	$R\bar{3}m$	-465 ^a	Γ_{15}	$P4mm$	-1104	R_{25}	$R\bar{3}c$	-2271
	M'_5	$Pmma$	-555 ^a	Γ_{15}, Γ_{25}	$Amm2$	-1254	$R_{25} + M_3$	$Pbnm$	-2312
GeTiO ₃	Γ_{25}	$P\bar{4}m2$	-0.5 ^a	M_3	$P4/mbm$	-444	$R_{25} + M_3$	$Cmcm$	-733 ^a
	Γ_{25}	$R32$	-1.5 ^a	R_{25}	$I4/mcm$	-455	$R_{25} + M_3$	$Pbnm$	-810
	R_{15}	$I4/mmm$	-314 ^a	R_{15}	$R\bar{3}m$	-501 ^a	Γ_{15}	$P4mm$	-854
	X'_5	$Pmma$	-328	R_{25}	$R\bar{3}c$	-589	Γ_{15}, Γ_{25}	$Amm2$	-881 ^a
	X'_5	$Cmcm$	-428	R_{15}, R_{25}	$Imma$	-704 ^a	Γ_{15}	$R3m$	-1053
SnTiO ₃	R_{15}	$I4/mmm$	-1.1 ^a	M_3	$P4/mbm$	-57	R_{15}, R_{25}	$Imma$ ^b	-84
	R_{15}	$R\bar{3}m$	-1.7 ^a	R_{25}	$I4/mcm$	-67	Γ_{15}	$R3m$	-240
	X'_5	$Pmma$	-21	R_{25}	$R\bar{3}c$	-74	Γ_{15}	$Amm2$	-242 ^a
	X'_5	$Cmcm$	-23	$R_{25} + M_3$	$Cmcm$	-78 ^a	Γ_{15}	$P4mm$	-291
PbTiO ₃	M_3	$P4/mbm$	-10.1	R_{25}	$R\bar{3}c$	-21.6	Γ_{15}	$Amm2$	-70.4 ^a
	R_{25}	$I4/mcm$	-19.6	R_{25}	$Imma$ ^b	-22.2	Γ_{15}	$P4mm$	-84.4
	$R_{25} + M_3$	$Cmcm$	-19.7 ^a	Γ_{15}	$R3m$	-66.3			

^aResults of additional calculations.

^bThe $Pbnm$ structure found in earlier calculations relaxes to the $Imma$ one.

TABLE IV. Frequencies of optical phonons at the Γ point in the cubic phase of $ATiO_3$ compounds (in cm^{-1}).

Compound	Source	TO1	TO2	TO3	LO1	LO2	LO3	Γ_{25}
MgTiO ₃	this work	260 <i>i</i>	151	649	106 <i>i</i>	372	905	191 <i>i</i>
CaTiO ₃	this work	165 <i>i</i>	176	607	122	407	857	93
	theor. ³	153 <i>i</i>	188	610	133	427	866	—
	theor. ¹³	140 <i>i</i>	200	625	136	428	864	130
SrTiO ₃	this work	68 <i>i</i>	162	549	152	428	792	202
	theor. ³	41 <i>i</i>	165	546	158	454	829	—
	theor. ⁶	100 <i>i</i>	151	522	146	439	751	219
	exp. ²⁹	—	175	544	172	475	796	—
BaTiO ₃	this work	151 <i>i</i>	175	471	172	439	683	269
	theor. ³	178 <i>i</i>	177	468	173	453	738	—
	theor. ⁸	195 <i>i</i>	166	455	162	434	657	266
	exp. ^{30 a}	—	181	487	180	468	717	306
RaTiO ₃	this work	212 <i>i</i>	172	444	166	434	638	287
ZnTiO ₃	this work	240 <i>i</i>	76	645	105 <i>i</i>	316	815	353 <i>i</i>
CdTiO ₃	this work	187 <i>i</i>	97	616	34	353	820	231 <i>i</i>
GeTiO ₃	this work	247 <i>i</i>	122	583	68 <i>i</i>	356	762	49 <i>i</i>
SnTiO ₃	this work	185 <i>i</i>	126	505	80	375	689	183
PbTiO ₃	this work	150 <i>i</i>	116	499	96	394	693	202
	theor. ³	144 <i>i</i>	121	497	104	410	673	—
	theor. ⁷	182 <i>i</i>	63	447	47	418	610	—

^aData for the tetragonal phase.

respectively) corresponding to the antiferroelectric distortions of the structure into the $Pmma$, $Cmcm$, and $P4/nmm$ phases. Among the unstable modes, the ferroelectric Γ_{15} mode is the most unstable and it determines the distortions observed in the crystal (the energies of three above-mentioned antiferroelectric phases are higher than that of the polar $P4mm$ phase). We note that the weaker phonon instability in our calculations as compared to the results of Ref. 9 is because our calculations were performed for the *theoretical* lattice parameter, whereas the calculations of Ref. 9 were performed for its *experimental* value. To illustrate the influence of the lattice strain on the phonon spectrum, the low-energy part of this spectrum calculated for the same lattice parameter as in Ref. 9 is shown in Fig. 1 by the dashed line.

The weak dependence of the unstable TO phonon frequency on the wave vector along the Γ - X - M - Γ path for vibrations polarized along the fourfold axes of the cubic structure was first discovered in Ref. 5. This dependence gives evidence for the dominant role of the vibrations in the ...-O-Ti-O-... linear chains oriented along these axes and for the weak interaction between adjacent chains.

A comparison of the phonon spectra of BaTiO₃ and RaTiO₃ shows that these spectra are very similar. In radium titanate, the most unstable mode is the Γ_{15} mode whose frequency depends only weakly on the wave vector along the Γ - X - M - Γ path. The instability of phonons in

TABLE V. Lowest phonon frequencies at high-symmetry points of the Brillouin zone in the cubic phase of $ATiO_3$ compounds (in cm^{-1}).

Compound	Source	Γ	X	M	R	Λ
MgTiO ₃	this work	260 <i>i</i>	190 <i>i</i>	314 <i>i</i>	315 <i>i</i>	246 <i>i</i>
CaTiO ₃	this work	165 <i>i</i>	32 <i>i</i>	215 <i>i</i>	226 <i>i</i>	122 <i>i</i>
	theor. ¹³	140 <i>i</i>	20	207 <i>i</i>	219 <i>i</i>	—
SrTiO ₃	this work	68 <i>i</i>	98	86 <i>i</i>	119 <i>i</i>	100
BaTiO ₃	this work	151 <i>i</i>	96 <i>i</i>	59 <i>i</i>	134	105
	theor. ⁸	219 <i>i</i>	189 <i>i</i>	167 <i>i</i>	128	—
RaTiO ₃	this work	212 <i>i</i>	182 <i>i</i>	158 <i>i</i>	110	87
ZnTiO ₃	this work	353 <i>i</i> ^a	319 <i>i</i>	437 <i>i</i>	424 <i>i</i>	337 <i>i</i>
CdTiO ₃	this work	231 <i>i</i> ^a	184 <i>i</i>	333 <i>i</i>	328 <i>i</i>	265 <i>i</i>
GeTiO ₃	this work	247 <i>i</i>	148 <i>i</i>	254 <i>i</i>	251 <i>i</i>	201 <i>i</i>
SnTiO ₃	this work	185 <i>i</i>	56 <i>i</i>	144 <i>i</i>	148 <i>i</i>	97 <i>i</i>
PbTiO ₃	this work	150 <i>i</i>	30	96 <i>i</i>	113 <i>i</i>	15 <i>i</i>
	theor. ⁷	182 <i>i</i>	31 <i>i</i>	35 <i>i</i>	145 <i>i</i>	58 <i>i</i>

^aThe Γ_{25} mode.

TABLE VI. Effective charges and optical dielectric constant for the cubic phase of $ATiO_3$ compounds.

Compound	Z_A^*	Z_{Ti}^*	$Z_{O\perp}^*$	$Z_{O\parallel}^*$	ϵ_∞
MgTiO ₃	2.537	7.773	-2.026	-6.258	7.01
CaTiO ₃	2.579	7.692	-2.085	-6.101	6.84
SrTiO ₃	2.561	7.725	-2.099	-6.088	6.87
BaTiO ₃	2.738	7.761	-2.186	-6.128	7.28
RaTiO ₃	2.764	7.789	-2.181	-6.192	7.42
ZnTiO ₃	3.233	8.257	-2.427	-6.637	11.64
CdTiO ₃	3.040	8.052	-2.300	-6.493	9.35
GeTiO ₃	4.460	7.572	-2.860	-6.314	10.49
SnTiO ₃	4.255	7.529	-2.745	-6.294	10.18
PbTiO ₃	3.931	7.623	-2.635	-6.283	9.34

TABLE VII. Elastic moduli of the cubic phase of $ATiO_3$ compounds (in GPa).

Compound	Source	C_{11}	C_{12}	C_{44}	B
CaTiO ₃	this work	388	100	91	196
	theor. ⁴	407	96	101	200
SrTiO ₃	this work	373	103	108	193
	theor. ⁴	388	104	117	199
	exp. ²⁷	316-348	101-103	119-124	174-183
BaTiO ₃	this work	338	110	123	186
	theor. ⁴	329	117	130	188
RaTiO ₃	this work	319	112	126	181
PbTiO ₃	this work	336	127	95	197
	theor. ⁴	334	145	100	208
	theor. ⁷	320	141	375?	203

RaTiO₃ is even more pronounced than in BaTiO₃. Taking into account the calculated energies of the distorted phases (Table III), we can suppose that RaTiO₃ is also a ferroelectric and that, as the temperature decreases, it undergoes three successive phase transitions as barium titanate does. The temperatures of these transitions are likely to exceed those in barium titanate. The values of the spontaneous polarization calculated by the Berry phase method in RaTiO₃ are also higher than those in BaTiO₃; they are 0.36 C/m² in the tetragonal phase and 0.41 C/m² in the rhombohedral phase. The calculated elastic moduli of the cubic RaTiO₃ are given in Table VII.

Now, we consider the phonon spectrum of CdTiO₃. This spectrum has a number of unstable modes at the X , M , and R points (X_3 , X_5 , X'_5 , M_3 , M'_5 , M'_2 , R_{25} , R_{15} modes) and two unstable modes at the Γ point. It is surprising that the main instability at the Γ point is due to the Γ_{25} mode associated with the deformation of the oxygen octahedron rather than to the ferroelectric Γ_{15} mode (see mode frequencies in Table IV). This deformation can result in the formation of the $P\bar{4}m2$, $Amm2$, and $R32$ phases, depending on the number of nonzero components of the order parameter.³⁵ The energy of the most stable of these phases ($R32$, Table III) is lower than the energy of the polar phases. Because of the qualitative similarity between the phonon spectra of calcium and cadmium titanates and between the eigenvectors of their unstable modes at the R and M points, CdTiO₃ can be considered as an analog of CaTiO₃ characterized by an even higher instability. Therefore, at room temperature, the structure of its nonpolar phase is $Pbnm$, as in the case of CaTiO₃. This conclusion was also made in Ref. 36. According to our data, the energy of this phase is lower than that of the cubic phase by 1.28 eV (Table III), which is somewhat higher than the value obtained in Ref. 36 (0.8 eV) and Ref. 10 (0.91 eV).

Although the ferroelectric instability associated with the Γ_{15} mode is not very important in the cubic CdTiO₃, it is known that this instability exists in the $Pbnm$ phase and results in the ferroelectric phase transition at 80 K. The first-principles calculations of the properties of the orthorhombic $Pbnm$ phase³⁶ did not find a stable ferroelectric distortion in it. In contrast, our calculations of the phonon spectrum at the Γ point of the orthorhombic CdTiO₃ reveal two unstable B_{1u} and B_{2u} modes resulting in the formation of polar $Pb2_1m$ and $Pbn2_1$ phases, respectively. These lattice distortions have been observed in X-ray studies of cadmium titanate at low temperatures.^{37,38} The properties of these phases will be considered in a separate paper.³⁹

The phonon spectrum of ZnTiO₃ is qualitatively similar to that of CdTiO₃, but it has an additional weak unstable M'_3 mode and is even less stable. The Γ_{25} mode in it is also less stable than the ferroelectric Γ_{15} mode (Table IV). However, as the most unstable modes in ZnTiO₃ are the R_{25} and M_3 ones, the $Pbnm$ phase has the lowest energy (Table III). The calculations of the phonon spectrum at the Γ point of the orthorhombic zinc titanate re-

veal two unstable B_{1u} and B_{2u} modes, which can cause the formation of the same polar phases as in cadmium titanate.

The phonon spectrum of MgTiO₃ is intermediate between those of zinc titanate and calcium titanate. It also has unstable Γ_{15} and Γ_{25} modes, but in magnesium titanate the ferroelectric Γ_{15} mode is less stable (Table IV). Nevertheless, as the phonons at the R and M points have the lowest frequency, the $Pbnm$ phase is the most energetically favorable (Table III). The calculations of the phonon spectrum at the Γ point in the orthorhombic magnesium titanate reveal one unstable B_{1u} mode, which can cause the $Pbnm \rightarrow Pbn2_1$ ferroelectric phase transition.

Finally, we discuss the phonon spectra of PbTiO₃, SnTiO₃, and GeTiO₃. The ferroelectric instability in these three compounds is associated with the Γ_{15} mode which competes with the unstable R_{25} and M_3 modes. From comparing the energies of different distorted phases (Table III), it follows that even in GeTiO₃, in which the unstable phonons at the Γ , R , and M points are close in frequency, the ferroelectric instability is dominant. The calculated spontaneous polarization is 1.28 C/m² in the tetragonal SnTiO₃ and 1.37 C/m² in the rhombohedral GeTiO₃. Our value of the spontaneous polarization in SnTiO₃ is significantly higher than the value of 0.73 C/m² obtained in Ref. 40. Among the perovskite compounds studied to date, GeTiO₃ is likely to have the highest spontaneous polarization.

It should be noted that in PbTiO₃ and SnTiO₃, the most energetically favorable phase is the tetragonal $P4mm$ phase, whereas in GeTiO₃ it is the rhombohedral $R3m$ phase. At the same time, the lattice strain in the tetragonal GeTiO₃ ($c/a = 1.1821$) is much higher than in lead titanate ($c/a = 1.0590$). This result calls into question the conclusion² that the stabilization of the tetragonal phase in PbTiO₃ is due to a high lattice strain (large c/a ratio).

V. DISCUSSION

As follows from Fig. 1, the phonon spectra of all $ATiO_3$ perovskite crystals studied in this work are characterized by several unstable modes, one of which is always the ferroelectric Γ_{15} mode. In the case where the R_{25} and M_3 modes competing with it have a lower frequency, the crystal undergoes distortions—the octahedra rotations, and its symmetry is lowered to $I4/mcm$ or $Pbnm$. The tendency toward such structural phase transitions increases with decreasing the A atom size.

From analyzing the characteristics of the Γ_{15} mode, one can draw a conclusion on the nature of the ferroelectric instability in studied crystals. As mentioned above, the dispersion law of this mode in BaTiO₃ and RaTiO₃ indicates strongly correlated motion of atoms along the ...-O-Ti-O-... chains. The analysis of the Γ_{15} phonon eigenvectors (Table VIII) shows that the A atoms do not

TABLE VIII. Eigenvectors of the dynamic matrix for an unstable TO1 phonon at the Γ point in the cubic phase of $ATiO_3$ compounds.

Compound	x_A	x_{Ti}	$x_{O\perp}$	$x_{O\parallel}$
MgTiO ₃	+0.6828	+0.1831	-0.4800	-0.1985
CaTiO ₃	+0.5693	+0.2391	-0.5225	-0.2696
SrTiO ₃	+0.3434	+0.3852	-0.5372	-0.3956
BaTiO ₃	+0.0299	+0.6734	-0.3561	-0.5404
RaTiO ₃	+0.0051	+0.6750	-0.2841	-0.6188
ZnTiO ₃	+0.5167	+0.1889	-0.5655	-0.2403
CdTiO ₃	+0.4012	+0.2358	-0.5919	-0.2875
GeTiO ₃	+0.5367	+0.1382	-0.5573	-0.2677
SnTiO ₃	+0.4177	+0.2123	-0.5670	-0.3709
PbTiO ₃	+0.2973	+0.2865	-0.5675	-0.4305

TABLE IX. Diagonal elements of the on-site force-constant matrix $\Phi_{xx}(0,0)$ for A and Ti atoms in the cubic phase of $ATiO_3$ compounds (in Ha/Bohr²).

Compound	A atom	Ti atom
MgTiO ₃	-0.0109	+0.1431
CaTiO ₃	+0.0163	+0.1370
SrTiO ₃	+0.0445	+0.1196
BaTiO ₃	+0.0755	+0.0873
RaTiO ₃	+0.0856	+0.0750
ZnTiO ₃	-0.0229	+0.1072
CdTiO ₃	-0.0008	+0.1113
GeTiO ₃	-0.0150	+0.0949
SnTiO ₃	+0.0132	+0.0786
PbTiO ₃	+0.0269	+0.0803

contribute much to the motion which is mainly determined by the out-of-phase Ti and O_{\parallel} displacements. As the size of the A atoms decreases, their contribution to the motion increases and becomes dominant, whereas the contribution of the Ti atoms decreases and the out-of-phase motion involves now not O_{\parallel} but O_{\perp} displacements. Thus, in crystals with small A atoms, the ferroelectric mode is determined by the out-of-phase displacements of the A atom and the cuboctahedron of oxygen atoms.

The values of the diagonal elements of the on-site force-constant matrix $\Phi_{xx}(0,0)$ for A and Ti atoms are presented in Table IX. These matrices are defined in terms of the restoring force acting on an atom displaced from its site, with the other atoms fixed at their lattice sites. To determine the on-site force constants from the force constants calculated using the ABINIT software for a sublattice displaced as a whole, the force constants calculated on a regular mesh of wave vectors were averaged.^{22,24,26} Positive values of the on-site force constants indicate that the position of an atom at its site is stable, while the negative values indicate that the atom is off-center. As

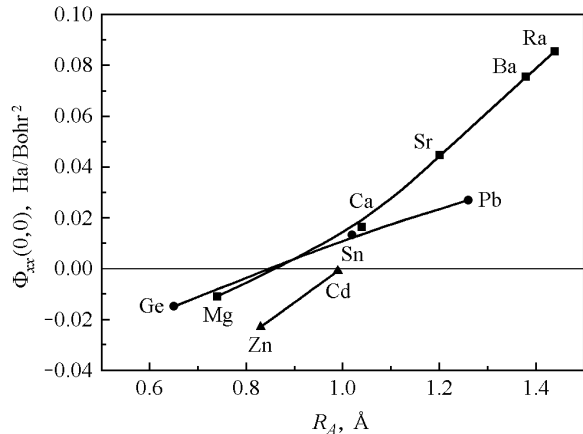


FIG. 2. Dependence of the $\Phi_{xx}(0,0)$ matrix element for the A atom on its ionic radius.

follows from Table IX, the off-centering of the A atoms should be observed in $ATiO_3$ perovskites for $A = Mg, Zn, Cd,$ and Ge . The $Sn, Ca,$ and Pb atoms are fairly close to the stability limit against the transition to an off-center position.

It should be recalled that in this work, the calculations were performed for the theoretical lattice parameter (corresponding to a minimum of the total energy). As the systematically underestimated lattice parameters in the LDA weakens the ferroelectric instability, many authors perform calculations for the experimental lattice parameters. In order to estimate the influence of this systematic error, we carried out a computer simulation which showed that an increase in the lattice parameter by 1% (which is a typical LDA error) decreases $\Phi_{xx}(0,0)$ in $PbTiO_3$ by 0.006 Ha/Bohr² for the A atom and by 0.016 Ha/Bohr² for the Ti atom. As a result, the atoms with $\Phi_{xx}(0,0)$ close to the stability limit against the transition to an off-center position can actually be off-center. Perhaps, this occurs in lead titanate, as indicated by extended X-ray-absorption fine-structure (EXAFS) studies.⁴¹

The main parameter determining the tendency of the A atom in $ATiO_3$ compounds to become off-center is its atomic size. However, if one plots the dependence of $\Phi_{xx}(0,0)$ on the ionic radius of the A atom (Fig. 2), it becomes clear that the curve for Zn and Cd atoms, as well as the curve for $Ge, Sn,$ and Pb atoms, are different from that for the “main” Mg – Ca – Sr – Ba – Ra series. This difference is likely a consequence of different configuration of the outer electron shell for the atoms. This configuration is d^{10} for Zn and Cd ; $d^{10}s^2$ for $Ge, Sn,$ and Pb ; and s^2p^6 for the atoms of the main series. The difference in the properties of these groups of atoms is clearly manifested in the Born effective charges of the A atoms (Table VI). Indeed, for the main series, the effective charge Z_A^* differs only slightly from the nominal charge of the cation (which indicates the predominantly ionic character of the

A–O bond); for the other two groups, the charge Z_A^* is significantly larger, which indicates that the bonding becomes more covalent in character.³

The obtained results suggest that off-center impurity atoms can exist in solid solutions of titanates with the perovskite structure. Since the average interatomic distance in these crystals is determined by the matrix, one can expect that the atoms for which $\Phi_{xx}(0, 0)$ has negative or small positive values can be off-center. Therefore, it is possible that the ferroelectric phase transition induced by Ca, Cd, and Pb impurities in SrTiO₃ (Ref. 12) is due to off-centering of these atoms. According to the EXAFS data, the Ba atoms in SrTiO₃ are on-center,⁴² but the Pb atoms in SrTiO₃ and BaTiO₃ can be off-center.⁴³

The results of this study differ somewhat from those obtained by Kvyatkovskii,¹¹ according to which the multiwell adiabatic potential occurred only for Mg and Zn atoms, whereas Cd atoms remained in the on-site positions. The discrepancy between our results is likely due to the fact that in Ref. 11 the calculations were performed for relatively small clusters in which the extended corre-

lation of atomic motion cannot be correctly taken into account (according to Refs. 5 and 8, the correlation length can be as large as 20 Å).

VI. CONCLUSIONS

The pseudopotentials constructed in this work have been used to calculate the phonon spectra of ATiO₃ perovskite crystals within the density functional theory. All known results on the structural instability in these compounds were reproduced and the properties of new, previously unknown systems were predicted. The analysis of the phonon spectra, the force constant matrix, and the eigenvectors of unstable TO phonons enabled to establish the relative contributions of the chain instability and off-centering of atoms to the appearance of ferroelectricity in these compounds. The main factors determining the possible off-centering of the *A* atoms are the geometric size of these atoms and the configuration of their outer electron shell.

-
- * swan@scon155.phys.msu.ru
- ¹ R. E. Cohen and H. Krakauer, Phys. Rev. B **42**, 6416 (1990).
 - ² R. E. Cohen, Nature **358**, 136 (1992).
 - ³ W. Zhong, R. D. King-Smith, and D. Vanderbilt, Phys. Rev. Lett. **72**, 3618 (1994).
 - ⁴ R. D. King-Smith and D. Vanderbilt, Phys. Rev. B **49**, 5828 (1994).
 - ⁵ R. Yu and H. Krakauer, Phys. Rev. Lett. **74**, 4067 (1995).
 - ⁶ C. LaSota, C.-Z. Wang, R. Yu, and H. Krakauer, Ferroelectrics **194**, 109 (1997).
 - ⁷ U. V. Waghmare and K. M. Rabe, Phys. Rev. B **55**, 6161 (1997).
 - ⁸ P. Ghosez, X. Gonze, and J.-P. Michenaud, Ferroelectrics **206–207**, 205 (1998).
 - ⁹ P. Ghosez, E. Cockayne, U. V. Waghmare, and K. M. Rabe, Phys. Rev. B **60**, 836 (1999).
 - ¹⁰ S. V. Halilov, M. Fornari, and D. J. Singh, Appl. Phys. Lett. **81**, 3443 (2002).
 - ¹¹ O. E. Kvyatkovskii, Phys. Solid State **44**, 1135 (2002).
 - ¹² V. V. Lemanov, in *Defects and Surface-Induced Effects in Advanced Perovskites* (Kluwer Academic Publishers, 2000) p. 329.
 - ¹³ E. Cockayne and B. P. Burton, Phys. Rev. B **62**, 3735 (2000).
 - ¹⁴ K. Parlinski, Y. Kawazoe, and Y. Waseda, J. Chem. Phys. **114**, 2395 (2001).
 - ¹⁵ The properties of one more member of this family of titanates, HgTiO₃, have been considered in Phys. Solid State **54**, 1663 (2012); DOI: 10.1134/S1063783412080185.
 - ¹⁶ X. Gonze, J.-M. Beuken, R. Caracas, F. Detraux, M. Fuchs, G.-M. Rignanese, L. Sindic, M. Verstraete, G. Zerah, F. Jollet, M. Torrent, A. Roy, M. Mikami, P. Ghosez, J.-Y. Raty, and D. C. Allan, Comput. Mater. Sci. **25**, 478 (2002).
 - ¹⁷ J. P. Perdew and A. Zunger, Phys. Rev. B **23**, 5048 (1981).
 - ¹⁸ A. M. Rappe, K. M. Rabe, E. Kaxiras, and J. D. Joannopoulos, Phys. Rev. B **41**, 1227 (1990).
 - ¹⁹ N. J. Ramer and A. M. Rappe, Phys. Rev. B **59**, 12471 (1999).
 - ²⁰ In this paper, the energy is measured in Hartrees (1 Ha = 27.2113845 eV) everywhere except Tables I and III.
 - ²¹ H. J. Monkhorst and J. D. Pack, Phys. Rev. B **13**, 5188 (1976).
 - ²² P. Giannozzi, S. de Gironcoli, P. Pavone, and S. Baroni, Phys. Rev. B **43**, 7231 (1991).
 - ²³ X. Gonze, Phys. Rev. B **55**, 10337 (1997).
 - ²⁴ X. Gonze and C. Lee, Phys. Rev. B **55**, 10355 (1997).
 - ²⁵ D. R. Hamann, X. Wu, K. M. Rabe, and D. Vanderbilt, Phys. Rev. B **71**, 035117 (2005).
 - ²⁶ X. Gonze, J.-C. Charlier, D. Allan, and M. Teter, Phys. Rev. B **50**, 13035 (1994).
 - ²⁷ *Landolt-Börnstein. Numerical data and functional relationships in science and technology. New Series. Group III.*, Vol. 36A1 (Springer-Verlag, 2001).
 - ²⁸ R. D. King-Smith and D. Vanderbilt, Phys. Rev. B **47**, 1651 (1993).
 - ²⁹ J. L. Servoin, Y. Luspain, and F. Gervais, Phys. Rev. B **22**, 5501 (1980).
 - ³⁰ T. Nakamura, Ferroelectrics **137**, 65 (1992).
 - ³¹ Our calculations show that the energy of the ilmenite phase of SnTiO₃, GeTiO₃, CdTiO₃, ZnTiO₃, and MgTiO₃ at $T = 0$ is lower than the energy of the most stable of the distorted perovskite phases. However, the energy difference between these phases is large enough (0.30–0.33 eV) only for the two last compounds.
 - ³² We use the mode notation introduced in Ref. 44.
 - ³³ In the case of SrTiO₃, despite the presence of the unstable R_{25} and M_3 modes in the phonon spectrum of the cubic

phase, the M_3 instability disappears when switching on the R_{25} rotations, and the energy of the $Pbnm$ phase (which relaxes to the $Imma$ phase) is 2 meV higher than that of the $I4/mcm$ phase.

- ³⁴ Further calculations have revealed two additional phases, $Cmcm$ and $Imma$, which are closer in energy to the ground state (Table V).
- ³⁵ The fact that the lattice symmetry is lowered to the polar $Amm2$ group follows from the transformation properties of the order parameter $(\eta, \eta, 0)$. The spontaneous polarization in this phase is 0.018 C/m^2 .
- ³⁶ G. Fabricius and A. L. García, Phys. Rev. B **66**, 233106 (2002).
- ³⁷ Y. J. Shan, H. Mori, R. Wang, W. Luan, H. Imoto, M. Itoh, and T. Nakamura, Ferroelectrics **259**, 85 (2001).
- ³⁸ Y. J. Shan, H. Mori, K. Tezuka, H. Imoto, and M. Itoh, Ferroelectrics **284**, 107 (2003).
- ³⁹ This paper has been published in Phys. Solid State **51**, 802 (2009); DOI: 10.1134/S1063783409040283. It has been shown that only the $Pbn2_1$ phase is stable at low temperatures; the other phase is suppressed by zero-point vibrations.
- ⁴⁰ Y. Konishi, M. Ohsawa, Y. Yonezawa, Y. Tanimura, T. Chikyow, T. Wakisaka, H. Koinuma, A. Miyamoto, M. Kubo, and K. Sasata, MRS Proc. **748**, U3.13 (2002).
- ⁴¹ N. Sicron, B. Ravel, Y. Yacoby, E. A. Stern, F. Dogan, and J. J. Rehr, Phys. Rev. B **50**, 13168 (1994).
- ⁴² V. Shuvaeva, Y. Azuma, K. Yagi, H. Terauchi, R. Vedrinski, V. Komarov, and H. Kasatani, Phys. Rev. B **62**, 2969 (2000).
- ⁴³ A. I. Lebedev, I. A. Sluchinskaya, A. Erko, A. A. Veligzhanin, and A. A. Chernyshov, Phys. Solid State **51**, 991 (2009).
- ⁴⁴ R. A. Cowley, Phys. Rev. **134**, A981 (1964).